Annual Technical Report 1993

Report Number: DE/ER/45391-4

"THEORY OF THE ELECTRONIC AND STRUCTURAL PROPERTIES OF SOLID STATE OXIDES"

Division of Materials Sciences

Office of Basic Energy Sciences

United States Department of Energy

Principal Investigator: Professor James R. Chelikowsky

Department of Chemical Engineering and Materials Science

University of Minnesota

Minneapolis, MN 55455

DISCLAIMER

Annual Technical Report 1993

Report Number DE/ER/45391-4

"Theory of the Electronic and Structural Properties of Solid State Oxides"

Principal Investigator: Professor J.R. Chelikowsky

1 Executive Summary of Research Accomplishments

This work has concentrated on the electronic and structural properties of solid state oxides. Emphasis has been on the electronic materials: silica, titania, and ruthenia. These are important materials in terms of their technological applications which range from the packaging of electronic devices to catalytic substrates. Fundamental interest has centered on the nature of the micro-structure of such solids in the amorphous state, or mixed oxide state.

New theoretical techniques have been implemented to examine such issues. The techniques outlined within this report are based on *ab initio* pseudopotential methods, and interatomic potentials.

Some areas examined under this project are: 1. The nature of the amorphization transformation of quartz under pressure. Specific focus is on the microscopic nature of the amorphous material and the driving forces for amorphization. 2. The equation of states of crystalline silica polymorphs. 3. Elastic anomalies in silica. In particular, the existence of a "negative" Poisson ratio in high temperature, low density forms of crystalline silica. 4. The optical and structural properties of titania and mixed oxides such as $Ru_xTi_{1-x}O_2$.

Highlights of this work includes:

• Proposal of a model of the structure of α-quartz under pressure [Physical Review Letters **65**, 3309 (1990); Nature **353**, 344 (1991); Phys. Rev. Letters **69**, 2220 (1992)]. A mechanism is proposed which accounts for changes in the coordination of silicon cations in silica under pressure. This mechanism is confirmed by direct calculations of the mechanical stability of α-quartz under pressure.

• Theoretical overview of the equations of state of silica [Physical Review B**44**, 1538 (1991); Physical Review B**44**, 4771 (1991); Physical Review B**44**, 4081 (1991);

Physical Review B **46**, 1 (1992)]. This overview permits the prediction for phase transition pressures for forms of crystalline silica.

• Confirmation of a negative Poisson ratio in α-cristobalite [Nature **358**, 222 (1992), and Phys. Rev. B (in press)]. This high temperature form of silica contracts in the transverse direction to a uniaxial strain. The work in this project was the first to explain this phenomena. It was also predicted that α-quartz will experience a negative Poisson ratio under uniaxial tension.

• Detailed theoretical analysis of the optical spectrum of titania and mixed oxides, specifically we have examined the $Ru_xTi_{1-x}O_2$ oxide system. [Solid State Communications **76**, 635 (1990); Phys. Rev. B **45**, 3874 (1992) and Phys. Rev. B (in press)].

2 PRIMARY RESEARCH ACCOMPLISHMENTS

A. The structure of amorphous silica under pressure

Pressure induced amorphization has been observed recently in a number of crystals[1, 2]. These solids vitrify when they are compressed at a sufficiently low temperature to inhibit crystallization. One of the most studied crystals is α-quartz. At pressures near ~25-35 GPa, quartz gradually transforms to an amorphous form[3]. Considerable interest exists in this direct crystal-to-amorphous transformation because of the technological potential for the production of bulk amorphous materials as well as their fundamental importance in geophysics. The question is whether computer "experiments" can give us insights into the origin of the driving force for this transformation, and the nature of structure of amorphous silica.

With respect to the driving force of the amorphization process, several suggestions have been made in the literature[4, 5]. One was that the crystal becomes unstable when its compressibility vanishes as demonstrated by molecular dynamical simulations[5]. However, this suggestion does not illuminate the physical origin of the transformation as any first order phase transformation would undergo such decrease in the compressibility. Another suggestion involved a softening of the elastic constants, but this suggestion is at variance with accurate theoretical calculations[3]. Neither suggestion focuses on the microscopic structure of quartz, and the physical basis of the transformation with respect to the chemical bond.

Amorphous materials are normally produced by the rapid cooling of a liquid. If the liquid quench is fast, then crystallization is prevented. Pressure induced amorphization is a more puzzling process, especially at ambient temperatures. For example, pressure induced amorphization in some situations can be reversible. Pressure amorphized $AlPO_4$ reverts to a quartz structure when the pressure is removed with the

same crystallographic orientationas before the amorphization[1]. Pressure amorphized silica remains amorphous upon the release of pressure, but the material is anisotropic having retained the "memory" of the original quartz crystallographic orientation[6].

In our calculations, we have followed the pressure evolution of quartz near and *above* the amorphization pressure. Our approach allows us to obtain information which is impossible to obtain from experiment, yet the results of our calculations can be as accurate as experiment. We use two approaches to understand the details of the amorphization process. Our first approach is to *ab initio* pseudopotentials to determine the elastic properties of quartz. This procedure is accurate, but computationally intensive. We complement this approach with simple, pairwise interatomic potentials. We establish the accuracy of the interatomic potential with the *ab initio* calculations. It is important that we do so as the mixed covalent and ionic components of the Si-O bond is not captured by pairwise forces, and *a priori* the covalent nature of the bond may be important when dealing with the quartz amorphization.

Our first principles calculations are performed within the LDA formalism using *ab initio* pseudopotentials and a plane wave basis[7]. We outline the essential features as the computational details have been presented elsewhere[8]. For the LDA, we use the exchange-correlation potential of Ceperley and Alder[9] as parameterized by Perdew and Zunger[10]. For the *ab initio* pseudopotentials we use norm conserving pseudopotentials as generated with the method of Troullier and Martins[11]. The diagonalization of the secular equation was handled via an iterative method[8]. Plane waves up to a kinetic energy of 64 Ry were included in the basis set in order to have sufficiently accurate forces for the structural properties. This cut-off was increased to 90 Ry for the stresses to determine the elastic properties. For α-quartz and most forms of crystalline silica, accurate structural energy calculations can be based on only one $\vec{k}$-point. Elastic constant calculations require more $\vec{k}$-points. For these calculations,

the Brillouin zone integrations were performed with a $\vec{k}$ point mesh of (2 x 2 x 2) with a displacement of $(0, 0, \frac{1}{4})$ in reciprocal lattice units. The $\vec{k}$ point mesh chosen has the unperturbed lattice symmetry which insures a commensurate transition from high-symmetry to low-symmetry lattices.

Our classical force-field calculations were based on the same functional form for the interatomic potentials used in previous simulations. The interactions in these pairwise potentials are described by a Coulomb term and two short ranged terms. These short ranged terms have the form of an attractive van der Waals term and a Born-Mayer correction, respectively. Results reported here employ two sets of parameters for this form: one from Tsuneyuki *et al.*[4], and one from van Beest *et al.*[12]. These potentials give a reasonable description of the structural properties of a number of silica polymorphs.

We will use both of these approaches to examine the mechanical instability of the quartz structure as a function of pressure. The elastic constants c_{ij} calculated here are those defined from the stress-strain relation, and those which appear in the equations of motion yielding the elastic-waves velocities. The c_{ij} are related to the energy variation to the second order in the strain[14]:

$$\frac{\Delta E^{(2)}}{V_o} = -p\frac{\Delta V^{(2)}}{V_o} + \frac{1}{2}\sum_{ij} c_{ij}\ \epsilon_i\ \epsilon_j$$

A symmetric strain tensor ϵ is assumed in Eq.(1), and we use Voigt's notation. $\Delta V^{(2)}/V_0 = \epsilon_1 + \epsilon_2 + \epsilon_3 + \epsilon_1\epsilon_2 + \epsilon_1\epsilon_3 + \epsilon_2\epsilon_3 + (\epsilon_4^2 + \epsilon_5^2 + \epsilon_6^2)/4$ is the relative volume change to the second order in strain.

A necessary condition for a crystal to be mechanically stable is that the elastic-wave energy be positive, or equivalently, that the elastic constant matrix be positive definite. This condition imposes the following constraints, the Born criteria:

$$B_1 = c_{11} - |c_{12}| > 0$$

$$B_2 = (c_{11} + c_{12})\, c_{33} - 2c_{13}^2 > 0$$

$$B_3 = (c_{11} - c_{12})\, c_{44} - 2c_{14}^2 > 0$$

for the crystal to be mechanically stable. The first criterion, B_1, insures stability with respect to the elastic waves in the xy-plane,*i.e.*, perpendicular to the quartz c–axis. The second condition, B_2, is related essentially to dilations, and insures a positive compressibility. The third condition, B_3, is associated with shear waves in planes different from the xy-plane. $B_3 = 0$ corresponds to a soft transverse acoustic mode with propagation and polarization vectors along one of the three equivalent directions in α-quartz, *e.g.*, the x direction, and along a direction $\tilde{y}$ in the yz plane at an angle $\beta = \arctan(-c_{44}/c_{14})$ of the c-axis.

In Figure 1, we illustrate the theoretical dependence of B_1, B_2, and B_3 for pressures up to 50 GPa. The experimental values at ambient pressure and a temperature of 4K are indicated by the arrows[13]. The zero-pressure elastic constants obtained from the *ab initio* pseudopotential calculations slightly overestimate the experimental results, an effect which we attribute to the minimal $\vec{k}$-point grid used in these heavy computations. The zero pressure values obtained with the interatomic potentials by Tsuneyuki, *et al.*[4], and by van Beest, *et al.*[12] are also presented in Figure 1. The *same* general pressure-dependence of the elastic constants is obtained with the pseudopotential and the interatomic potentials.

The first two moduli, B_1 and B_2 are positive over the pressure range illustrated and increase at high pressure. The change in the shear modulus is relatively small. B_2 increases drastically over the same range; it changes by one order of magnitude from ambient pressure to 50 GPa. The striking increase in B_2 is related to the decrease with pressure of the α-quartz compressibility. It reflects the increasing stiffness of the Si-O-Si angle owing to the Si-Si repulsion, when the bond-bending approaches 120°.

The quartz instability is associated with the third Born criteria, B_3. In Figure 1, B_3

decreases with pressure and becomes negative near 30 GPa. The transition pressure for instability differs somewhat between the interatomic potentials and the pseudopotential calculation, but all three calculations indicate an instability near ~20-35 GPa. The mechanical instability is consistent with the structural transformation observed in molecular dynamics simulations. Contrary to what might be extrapolated from the low pressure behavior of the elastic constants[3], neither $c_{66} = \frac{1}{2}B_1$, nor c_{44} vanish in the region of quartz amorphization. c_{66} *increases* above 10 GPa and c_{44} vanishes only at pressures above ~50 GPa, far above the instability in B_3. Based on these interatomic potentials, and our pseudopotential calculations, it is clear that the vanishing of c_{66} and c_{44} are not the cause of the mechanical instability.

The pair potentials and pseudopotential approaches differ quantitatively with respect to the pressure scale. However, both approaches reveal the same microscopic origin of the quartz instability. The violation of the stability condition, B_3 occurs when the oxygen anions approach a bcc configuration[15]. This packing is the dominant mechanism which controls the structural behavior of quartz at high pressure. Since this bcc oxygen arrangement is a "Madelung", or "coulombic" effect, resulting from the minimization of the oxygen-oxygen repulsion, it is reasonable that a simple pairwise interatomic potential would replicate the microscopic origin of the instability.

The angle β between the c-axis and the $\tilde{y}$ axis yielding the soft shear, $\epsilon_{x\tilde{y}}$ is about 40° at the transition pressure and decreases slightly at higher pressures. This angle saturates at about 35° when the bcc packing is nearly completed (near 50 GPa). The corresponding shear, $\epsilon_{x\tilde{y}}$ has a simple interpretation in the bcc lattice. In Figure 2, we illustrate the connection between the quartz hexagonal basis vectors ($\vec{a}$,$\vec{b}$,$\vec{c}$) and the oxygen cubic cell. The quartz structure can be composed of 27 of these "oxygen sublattice" bcc cells as the silicon cations are not equivalent in each subcell. For $\beta = \arccos(\sqrt{2/3}) \simeq 35.3°$, the $\epsilon_{x\tilde{y}}$ shear is ideally parallel to one of the three sets of planes forming the faces of the bcc

cell. The x and $\tilde{y}$ directions are face-diagonals of the cell. The effect of the strain is to elongate the bcc sublattice. In Figure 3, we compare the microscopic atomic arrgangment obtained from the *ab initio* pseudopotential calculations in the unstrained quartz structure and in the strained structure. Microscopically, the effect of the elongated bcc sublattice is to alter the O-Si-O angles. The angles which have oxygen anions along the elongation axis are opened; those with anions perpendicular to the axis are closed. This deformation produces a displacement of the silicon cations towards one of the nearby octahedral sites in the bcc lattice. The same effect is found in the interatomic potential calculations. This displacement increases with pressure and is clearly related to the shear-instability.

While these calculations can yield insights into the driving forces of the amorphization process, they are clearly limited as we restrict the calculations to the *quartz structure.* At this point, all that one can state is that the quartz structure is unstable. If we were restricted in our knowledge of the experimental details, all we could say was that quartz might transform to another structure. This structure could be a small deformation of the quartz structure, another crystalline form, or it could be an amorphous solid. By employing *molecular dynamics*, we can gain some insights into the transformation which cannot be obtained by *static* deformations. Molecular dynamics will allow us to follow the instability of quartz to another structure. It should be noted that this procedure may not result in a quantitative understanding of the amorphization procedure. The molecular dynamics calculations will not be on an experimental time scale. Also, owing to the intensive computational cost of *ab initio* molecular dynamics calculations we resort to simple pairwise potentials to describe the interatomic forces in these simulations. These potentials are not as reliable as the pseudopotential calculations and the resulting strtucture may not be quantitatively correct.

In our *preliminary* simulations for the amorphization transformation, we used the interatomic potentials from van Beest, *et al.*[12]. Our simulation was performed at constant

pressure using the variable shape cell simulation of Wentzcovitch[16]. While the details of the simulation are somewhat dependent on the choice of the time step, and other technical aspects of the calculation, several feature of the amorphization transformation seem clear. First, we find the oxygen arrangement during and after the transformation resembles a distorted bcc sublattice, *e.g.*, the radial distribution of the pressure induced amorphized silica shows an average O-O coordination of eight. We find the silicon cations occupy mixed 4- and 6-fold coordinated sites as one would expect on the basis of the shear instability illustrated in Figure 3. Also, we find that the transformation is first order with a density increase of $\sim$15%.

In Figure 4, we illustrate the quartz structure before the amorphization transformation. In Figure 5, we illustrate the simulated amorphous silica structure. The amorphous structure in Figure 5 may not be quantitave in terms of structural details, but it illustrates how computer simulations can give microscopic structural details which are simply not accessible from experiment.

B. Mixed oxides: $\mathbf{Ru}_x\mathbf{Ti}_{1-x}\mathbf{O}_2$

Significant advances have been made both theoretically and experimentally in our ability to modify the electronic properties of semiconductors through doping and/or alloying. While "band-gap engineering" is well known in the semiconductor industry, its application to transition-metal oxides resides in a more primitive stage. Notwithstanding, the electronic modification of these materials is becoming increasingly important for a number of technological applications. Unlike semiconductors, few theoretical investigations have been performed for transition-metal oxides. Traditionally, oxides have been one of the most difficult classes of solids upon which to perform "first-principles" pseudopotential calculations owing to the localized nature of the transition-metal d and O $2p$ valence wave functions[17,

18]. However, with the recent advances in techniques for generating "soft-core" transferable pseudopotentials,[19, 20] and fast iterative diagonalization techniques,[21] we are now in a position to handle these complex systems from first-principles.

As a first step towards "band-gap engineering" for transition-metal oxides using *ab initio* calculations, we have chosen to study the $Ru_xTi_{1-x}O_2$ system owing to its use in energy-storage and conversion processes[22–24], the photocatalytic treatment of waste-water[25], anti-chalking agents in the paint and polymer industry[26], as a catalyst in the photo-methanation of carbon dioxide[27], and as an electrocatalyst in the chlor-alkali industry[28, 29]. These applications depend upon the transfer of electrons (holes) from the conduction (valence) band to a reactant molecule or electrolyte after the electro/photo excitation process. The reaction pathways at the surface are often complex. An understanding of the bulk electronic properties for these mixed oxide systems, and the location of impurity states will aid in the design of better catalysts and electro-optic devices. An example of the impact of "band-gap engineering" in transition-metal oxides is illustrated by the production of H_2 through band-gap illumination of TiO_2 electrodes[22]. The difficulty with this process however, lies in the 3.05 eV band gap[30] found in pure TiO_2. This large gap results in photon absorption near the uv region of the spectrum where solar photon fluxes are small. By doping TiO_2, it is hoped that the absorption spectrum may be shifted to longer wavelengths through the formation of induced states within the fundamental band gap thereby making TiO_2 an attractive material for energy-storage and conversion processes.

Although the electronic properties of TiO_2 have been extensively studied in the literature,[17] and to a lesser extentfor RuO_2[18], little is known theoretically about the $Ru_xTi_{1-x}O_2$ system. We employed *ab initio* calculations performed within the local-density approximation for the quasibinary $Ru_xTi_{1-x}O_2$ oxide using a plane-wave basis and "soft-core" pseudopotentials[19]. We have shown this methodology to give good results[17, 18]

for the electronic, structural, and optical properties of the end member oxides: TiO_2 and RuO_2. Our Ti, Ru, and O pseudopotentials were generated by the method Troullier and Martins[19] as previously described.[17, 18] We focused upon the symmetry and location of Ru induced impurity states relative to the valence-band edge of crystalline TiO_2 by examining the $Ru_xTi_{1-x}O_2$ system as $x \rightarrow 0$.

We have performed total-energy pseudopotential calculations for ideal $Ru_xTi_{1-x}O_2$ solid solutions at $x = 0$, $1/24$, $1/4$, $1/2$, $3/4$, and 1. We employed supercells with the appropriate number of Ru atoms substituted for Ti. At $x = 1/2$, we used a $1 \times 1 \times 1$ cell, at $x = 1/4$, and $3/4$, a $1 \times 1 \times 2$ supercell, and at $x = 1/24$, a $2 \times 2 \times 3$ supercell. While lattice rearrangement is possible, we found no significant modifications from the tetragonal symmetry of our supercells. In fact, solid solution behavior might be expected for $0 < x < 1$ as both Ru^{4+} and Ti^{4+} have similar ionic radii, electronegativities, and both oxides occur in the rutile structure with similar lattice constants. At each concentration, excluding $1/24$ which will be discussed below, we have minimized the the total energy with respect to the tetragonal lattice constants a, and c, and the atomic positions of the the Ru, Ti, and O atoms. The number of special **k** points was increased until convergence in the total-energy of 0.05 eV per formula unit of $Ru_xTi_{1-x}O_2$, or better, was obtained. For $x = 0$ we have used one special **k** point, eight for $x = 1/4$, $1/2$, $3/4$, and six points for $x = 1$. Calculations were performed with a 64 Ry plane-wave cutoff resulting in total energies which were converged to 0.05 eV/atom or better for the end member oxides.

In Fig. 6, we show the resulting density of states (DOS) for $x = 1/4$ along with the TiO_2 and RuO_2 end member oxides. The DOS was calculated using the analytic tetrahedron method[31] using the self-consistent solution at 126 **k** points in the irreducible Brillouin zone. The DOS for TiO_2 and RuO_2 have been discussed previously[17, 18]. The Fermi energy was taken as the energy zero in each panel while occupied states are indicated by shading. Valence band states between -9 to -1 eV are predominately O $2p$ states while

those greater than -1 eV are predominantly Ti $3d$ and Ru $4d$ states in analogy with the t_{2g} and e_g states of an octahedrally coordinated transition-metal ion in the presence of a crystal field. For $0 < x < 1$ the width of the O $2p$ manifold monotonically increases with x resulting in a separation of $\sim$ 1 eV between end members while the separation between the top of the O $2s$ (not shown), and the bottom of the O $2p$ manifold monotonically decreases by $\sim$ 1 eV between end members. At these concentrations we find the heat of mixing for the orderd oxides to be positive, i.e., unstable, in agreement with experiment[33].

The substitution of Ru for Ti results in an attractive potential for the additional electrons originating from the atomic Ru $4d$ states. This attractive potential subsequently lowers states in the t_{2g}-e_g manifold. For $x << 1$ one expects localized Ru $4d$ states in the vicinity of the TiO_2 fundamental gap as experimentally observed[32] for V, Cr, Fe, and Mn dopants in TiO_2. At higher Ru concentrations, these localized states will tend to overlap due to the decreasing Ru-Ru distance and eventually lead to metallic character as the t_{2g} and e_g complexes are pulled down towards the O $2p$ manifold as seen in Fig. 6. For $x = 1/4$, the Ru induced impurity states occupy the fundamental TiO_2 band gap as seen in Fig. 6. The width of the impurity complex is $\sim$ 1 eV and is separated from the valence-band and conduction-band edges by a gap of $\sim$ 1/2 eV. From our band structure calculations we find this midgap feature to be composed of three states. As the charge state of Ru in $Ru_xTi_{1-x}O_2$ has been experimentally determined[33, 34] from Mössbauer absorption spectra to be almost exclusively Ru^{4+} ($4d^4$), one expects two filled defect bands (excluding spin) associated with the substitutional Ru. Overall, the DOS for the $x = 1/4$ binary oxide remains similar to that of the undoped crystal shown in the bottom panel of Fig. 6. Recent x-ray photoelectron spectroscopic experiments have been performed for electrochemically active RuO_2-TiO_2/Ti overlayers[35] containing $\sim$ 20 mol% RuO_2. A comparison between our theoretical results and the experimental XPS spectra of the $Ru_{0.19}Ti_{0.81}O_2$ films is given in the center panel of Fig. 6. Overall, our theoretical valence band features are in

good agreement with the experimental spectra given the morphological and stoichiometric differences. As the concentration is increased, we find the Ru midgap states overlap with the t_{2g}-e_g manifold at $x \sim 0.4$

The exact location of Ru states however, is difficult to asses in the case of $x = 1/4$ as the width of the defect complex is $\sim$ 60% of the TiO_2 band gap. Further, these Ru induced states become difficult to probe experimentally owing to surface and defect states lying in the fundamental gap[36, 34]. The variability of the transition metal valence charge leads to further difficulties in determining whether these states are donors or acceptors when optical experiments are employed. Theoretically, the position of these defect states are determined by calculating the electronic structure of the alloy in the infinatly dilute limit. For semiconductors, however, the problem is difficult to treat using a supercell geometry as defect-defect interactions lead to a significant dispersion of these states unless very large supercells are employed. Owing to the localized nature of the transition-metal d and O $2p$ wave functions, much smaller supercells may be used in comparison to e.g. Si:P. As the Ru induced states have already localized in the band gap by $x = 1/4$ as seen in Fig. 6, we have modeled the TiO_2:Ru system by using a Ru concentration of $x = 1/24$ with a $2 \times 2 \times 3$ supercell containing 72 atoms. At this concentration the minimum Ru-Ru separation is a factor of two larger than $x = 1/4$. As in the case of TiO_2, one special $\mathbf{k}$ point was used to sample the charge density. The lattice constants for the tetragonal supercell were based on TiO_2 as experimental x-ray diffraction experiments[37] for $x \leq 0.02$ found differences of only 1-3% from those of TiO_2. To ease the computational burden, the plane-wave cutoff was reduced from 64 Ry to 40 Ry as the band structure converges much faster than the total energy. We have tested the 40 Ry cutoff for crystalline TiO_2 finding relative shifts in the band structure on the order of 0.1 eV.

To estimate the location of Ru induced impurity bands relative to the top of the O $2p$ manifold for TiO_2:Ru, band structure calculations were performed for $x = 1/24$. In Fig. 7

we show the three Ru induced gap states along various high symmetry directions of the tetragonal BZ where the Fermi energy has been taken as the energy zero. In this figure, the filled O $2p$ valence states are indicated by shading while only the bottom of the conduction bands are shown. The band width of the Ru induced defect states was found to be 0.37 eV while the difference between the top of the O $2p$ valence band states and the bottom of the Ti t_{2g} states remains essentially unchanged from the LDA value of 2.02 eV for pure TiO_2. Comparing the band width at a doping of $x = 1/4$ of 1.2 eV, the defect induced band width at $x = 1/24$ has decreased by a factor of approximately three upon doubling the the minimum Ru-Ru separation. The center of gravity of the Ru induced complex is approximately 1 eV above the O $2p$ manifold. Ultraviolet photoelectron spectroscopic experiments performed by Triggs[34], for single crystals doped with 2% Ru resulted in a valence band similar to the undoped TiO_2 spectra. While this Ru doping is close to our Ru concentration of $x = 1/24$, variations in surface stoichiometry and a large depletion layer width make it difficult to assign features to bulk spectra.[34] These experiments did however reveal a shift in valence band edge into the fundamental TiO_2 band gap corresponding to occupied Ru $4d$ impurity states. A more direct comparison of the location of the impurity induced Ru states to experiment is obtained from single crystal optical absorption spectra by Triggs.[34] For crystals doped with 2% Ru, a shift in the fundamental absorption edge from 3.05 eV[30] to 1.85 eV was observed. Gutiérrez and Salvador[38] have performed photoelectrochemical experiments on $Ru_{0.03}Ti_{0.97}O_2$ single crystals revealing two distinct transitions. The first transition occurring at 3.2 eV corresponding to electron transfer from the top of the O $2p$ manifold to the lower edge of the Ti $3d$ states and a 2 eV transition corresponds to electron transfer from the Ru $4d$ states to the lower edge of the the Ti $3d$ states. Both experiments result in an $\sim$ 1.2 eV separation between the top of the O $2p$ manifold to the narrow defect band and are in good agreement with our theoretical predictions.

Pseudocharge density contour plots for defect states in high symmetry planes of the tetragonal lattice for $x = 1/24$ are shown in Fig. 8. We have indicated the Ti-O "bonding network" in the $2 \times 2 \times 3$ supercell by solid lines, and have placed the single Ru impurity in the center of each plane. In panel (a), we show the (110) plane for the lowest band of $d_{x^2-y^2}$ like symmetry, panel (b) shows the second band in the $(\bar{1}10)$ plane of d_{zy} symmetry, and panel (c) shows the third defect band in the (001) plane of d_{zx} symmetry. The symmetry of these states have been taken from the splitting of the five Ru atomic d states in the presence of an octahedron of O^{2-} ions as the distortion from O_h to D_{2h} symmetry is small[18]. From Fig. 8 it is clear that the three defect induced gap states are localized on the Ru atoms with a small amount of O $2p$ character associated with the $pd\pi$ t_{2g} bonds occurring between the nearest neighbor O^{2-} ions.

To summarize, we have found that Ru doping of TiO_2 results in three defect bands occurring in the fundamental gap. The character of these defect states has has been determined from pseudocharge density plots to be localized atomiclike Ru $4d$ states of t_{2g} like symmetry. The location of these defect states was found to be ~ 1 eV above the O $2p$ manifold, in agreement with experimental results.

REFERENCES

[1] M.B. Kruger and R. Jeanloz, Science **249**, 647 (1990), and references therein.

[2] G.C. Serghiou, R.R. Winters and W.S. Hammack, Phys. Rev. Lett. **68**, 3311 (1992) and references therein.

[3] R.J. Hemley, A.P. Jephcoat, H.K. Mao, L.C. Ming, and M.H. Manghani, Nature **334**, 52 (1988).

[4] S. Tsuneyuki, Y. Matsui, H. Aoki, and M. Tsukada, Nature **339**, 209 (1989).

[5] J.S. Tse and D.D. Klug, Phys. Rev. Lett. **67**, 3559 (1991).

[6] L.E. McNeil and M. Grimsditch, Phys. Rev. Lett. **68**, 83 (1992).

[7] J.R. Chelikowsky and M.L. Cohen, "*Ab initio* Pseudopotentials and the Structural Properties of Semiconductors", *Handbook on Semiconductors*, editor by P.T. Landsberg, (Elsevier, Amsterdam, 1992), p. 59.

[8] J.R. Chelikowsky, N. Troullier, J.L. Martins, and H.E. King, Jr., Phys. Rev. B **44**, 489 (1991); N. Binggeli, N. Troullier, J.L. Martins, and J.R. Chelikowsky, Phys. Rev. B **44**, 4771 (1991) and N. Binggeli and J.R. Chelikowsky, Phys. Rev. Lett. **69**, 2220 (1992).

[9] D.M. Ceperley and B.J. Alder, Phys. Rev. B **45**, 566 (1980).

[10] J.P. Perdew and A. Zunger, Phys. Rev. B **23**, 5048 (1981).

[11] N. Troullier and J.L. Martins, Phys. Rev. B **43**, 1993 (1991).

[12] B.W.H. van Beest, G.J. Kramer and R.A. van Santen, Phys. Rev. Lett. **64**, 1955

(1990).

[13] A.G. Smagin and B.G. Mil'shtein, Soviet Physics Crystallogr. **19**, 514 (1975).

[14] We use the notation: $\epsilon_1 = \epsilon_{xx}, \epsilon_2 = \epsilon_{yy}, \epsilon_3 = \epsilon_{zz}, \epsilon_4 = 2\epsilon_{yz}, \epsilon_5 = 2\epsilon_{zx}$, and $\epsilon_6 = 2\epsilon_{xy}$.

[15] N. Binggeli and J.R. Chelikowsky, Nature **353**, 344 (1991).

[16] R. Wentzcovitch and J.L. Martins, Solid State Comm. **78**, 831 (1991).

[17] K. M. Glassford and J. R. Chelikowsky, Phys. Rev. B **46**, 1284 (1992).

[18] K. M. Glassford and J. R. Chelikowsky, Phys. Rev. B **47**, xxx (1993).

[19] N. Troullier and J. L. Martins, Phys. Rev. B **43**, 1993 (1991).

[20] A. Rappe, K. Rabe, E. Kaxiras, and J. D. Joannopoulos, Phys. Rev. B **41**, 1227 (1990); D. Vanderbilt, Phys. Rev. B **32**, 8412 (1985).

[21] J. L. Martins and M. L. Cohen, Phys. Rev. B **37**, 6134 (1988); J. L. Martins, N. Troullier, and S. -H. Wei, *ibid* **43** 2213 (1990).

[22] A. Fujishima and K. Honda, Bull. Chem. Soc. Japan **44**, 1148 (1971); *ibid.* Nature **238**, 37 (1972).

[23] J. Manassen, D. Cahen, G. Hodes, and A. Sofer, Nature **263**, 97 (1976).

[24] B. O'Regan and M. Grätzel, Nature **353** 737, (1991).

[25] F. Sabin, T. Türk, and A. Vogler, J. Photochem. Photobiol. A: Chem, **63** 99 (1992).

[26] Z. Luo and Q.-H. Gao, J. Photochem. Photobiol. A: Chem, **63** 367 (1992).

[27] K. R. Thampi, J. Kiwi, and M. Gratzel, Nature **327**, 506 (1987).

[28] S. Trasatti, and W. E. O'Grady, *Advances in Electrochemistry and Electrochemical Engineering*, ed. H. Gerischer and C. W. Tobias, Vol. 12, (Wiley-Interscience, New York, 1981) p. 177; S. Trasatti, p. 225 (1991).

[29] D. M. Novak, B. V. Tilak, and B. E. Conway, *Modern Aspects of Electrochemistry*, Vol. 14, ed. J. O'M. Bockris, B. E. Conway and R. E. White (Plenum Press, New York, 1982), p. 195.

[30] J. Pascual, J. Camassel, and H. Mathieu, Phys. Rev. Lett. **39**, 1490 (1977); Phys. Rev. B **18**, 5606 (1978).

[31] G. Lehmann and M. Taut, Phys. Status Solidi **54**, 469 (1972); O. Jepsen and O. K. Anderson, Solid State Commun. **9**, 1763 (1971).

[32] K. Mizushima, M. Tanaka, A. Asai, S. Iida, and J. Goodenough, J. Phys. Chem. Solids **40**, 1129 (1979)

[33] P. Triggs, F. Levy, and F. E. Wagner, Mater. Res. Bull. **19**, 197 (1984).

[34] P. Triggs, Helv. Phys. Acta **58**, 657 (1985).

[35] N. Wagner and L. Kühnemund, Cryst. Res. Technol, **24**, 1009 (1989).

[36] V. E. Henrich, G. Dresselhaus, and H. J. Zeiger, Phys. Rev. Lett. **36**, 1335 (1976); A. K. See and R. A. Bartynski, J. Vac. Sci. Technol. A**10**, 2591 (1992.

[37] P. Triggs, H. Berger, C. A. Georg and F. Levy, Mater. Res. Bull. **18**, 677 (1983).

[38] C. Gutiérrez and P. Salvador, J. Electroanal. Chem. **187**, 139 (1985).

[39] Z. Zhang, S.-P. Jeng, and V. E. Henrich, Phys. Rev. B **43**, 12004 (1991).

[40] G. van der Laan, Phys. Rev. B **41**, 12366 (1990).

[41] J. Riga, C. Tenret-Noël, J. J. Pireaux, R. Caudano, and J. J. Verbist, and Y. Gobillon, Phys. Scr. **16**, 351 (1977).

FIGURES

FIG. 1. Pressure dependence of the Born elastic moduli as defined in the text: (a) $B_1 = c_{11} - |c_{12}|$, (b) $B_2 = (c_{11} + c_{12})c_{33} - 2c_{13}^2$, and (c) $B_3 = (c_{11} - c_{12})c_{44} - c_{14}^2$. The pseudopotential results are given by the filled circles. The interatomic potential results are given by open circles and fille squares.

FIG. 2. Soft shear $\epsilon_{x\tilde{y}}$ on the oxygen body centered cubic (bcc) sublattice in the quartz high-pressure structure. The Si cations are not equivalent in the small oxygen bcc cells; 27 of these cells are needed to form a periodic cubic cell of quartz. The hexagonal basis vectors ($\vec{a}$, $\vec{b}$, $\vec{c}$) of quartz correspond to two face diagonals and a body-diagonal of the cube, respetively.

FIG. 3. Projection of the atomic arrangement in the quartz high-pressure unstrained structure (left hand side) and in high-pressure strained structure (right hand side). The high-pressure bcc model of quartz and the tetrahedral and octahedral sites in the oxygen bcc lattice are illustrated in the upper section of the figure. The strain produces a displacement of the silicon cations toward one of the nearby octahedral sites.

FIG. 4. A "ball and stick" model of the quartz structure. The silicon atoms are depicted by the green spheres; the oxygen atoms are red spheres. This supercell is used to simulate the amorphization transformation, 243 atoms are contained within the cell.

FIG. 5. A "ball and stick" model of pressure amorphized quartz. The silicon atoms are

depicted by the green spheres; the oxygen atoms are red spheres. Note how some of the silicon atoms are in six-fold sites, while others are in four-fold sites.

FIG. 6. Density of states for $Ru_xTi_{1-x}O_2$ for various Ru concentrations compared to experimentally determined spectra (see text for referencs). The Fermi energy has been taken as the energy zero.

FIG. 7. Band structure of $Ru_xTi_{1-x}O_2$ with $x = 1/24$.

FIG. 8. Pseudocharge density plots for three characteristic Ru induced defect states for $x = 1/24$ shown in symmetry planes revealing the Ru atomic-like $d-$character.

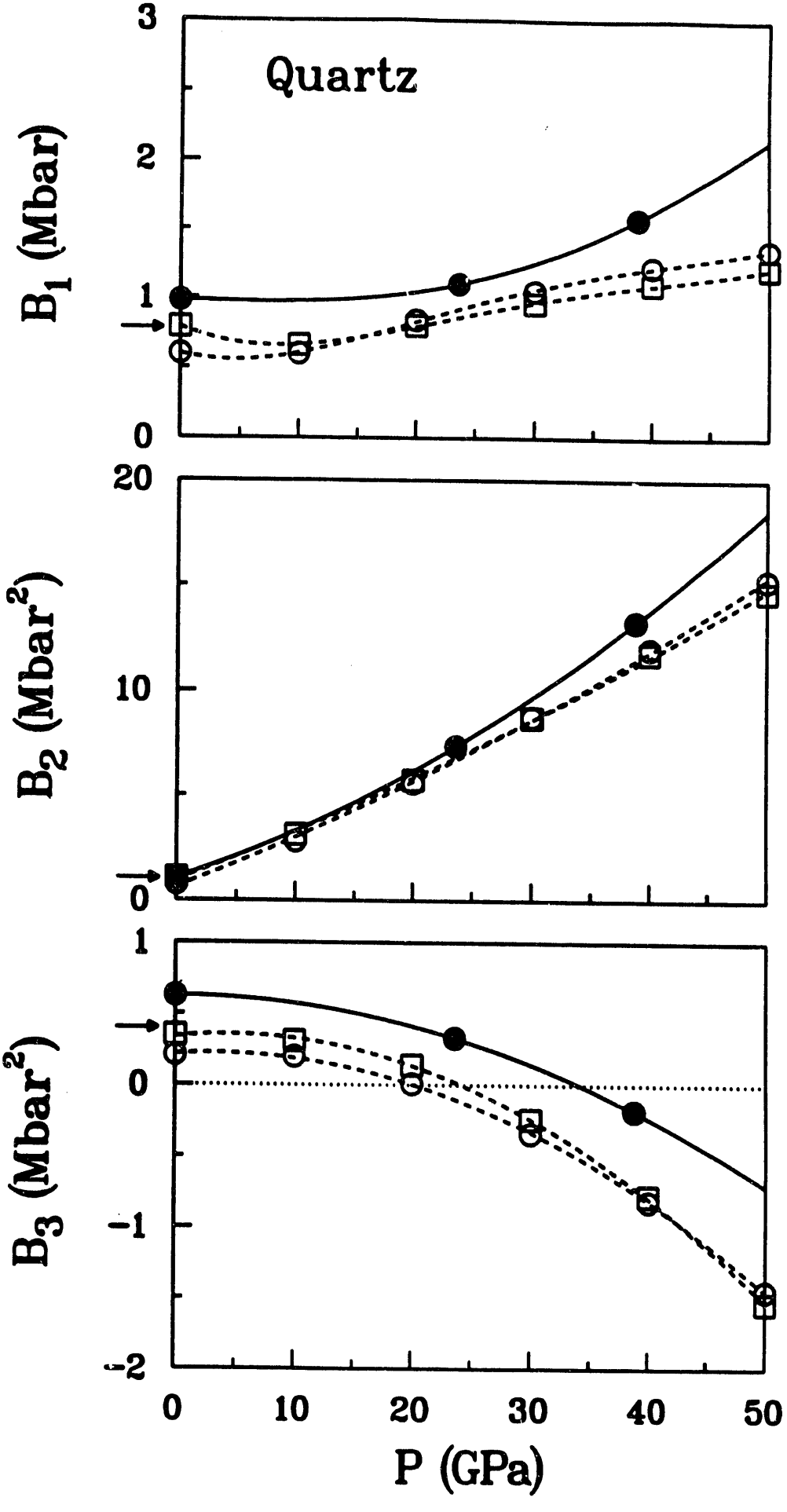
Quartz
B_1 (Mbar)
B_2 (Mbar^2)
B_3 (Mbar^2)
P (GPa)
3
2
1
0
20
10
0
1
0
-1
-2
0
10
20
30
40
50

Fig 1

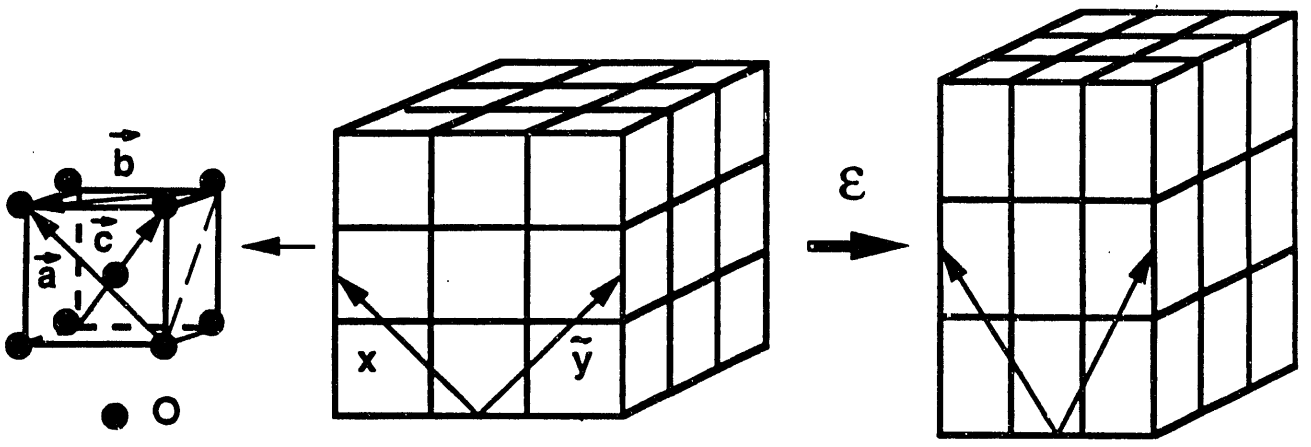

Fig 2

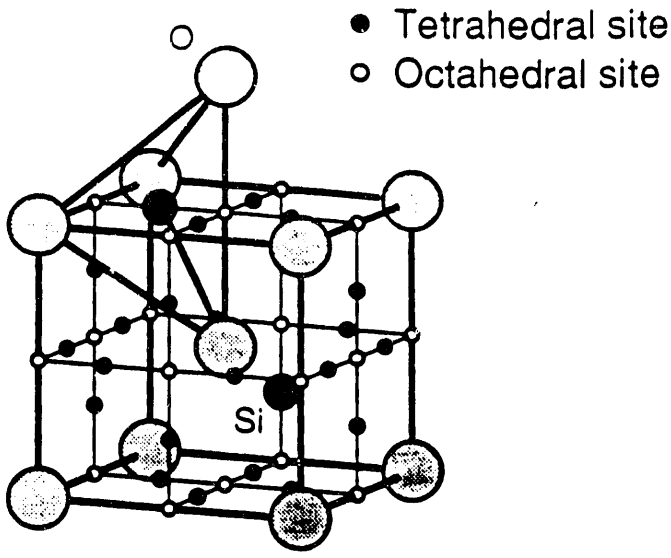

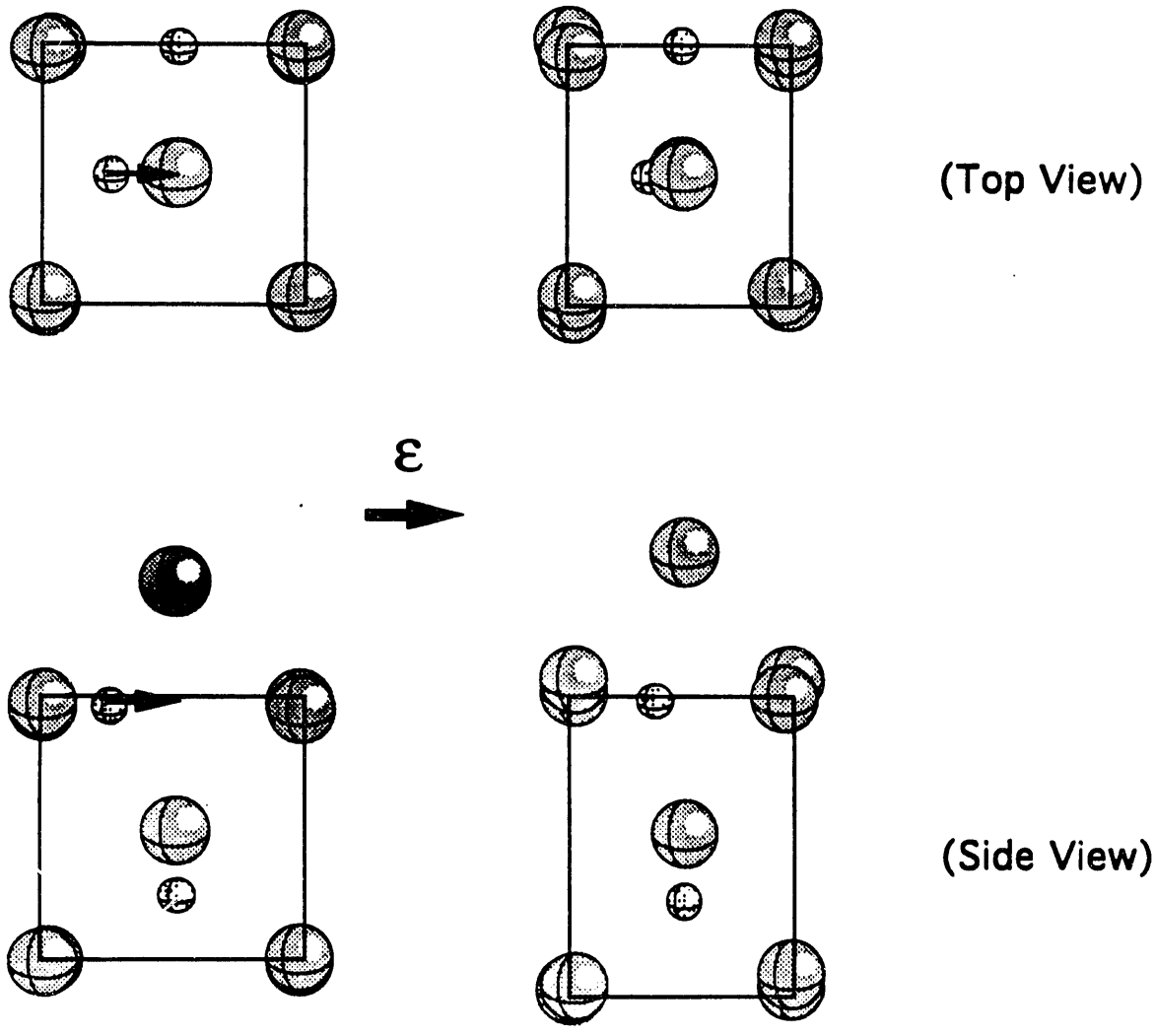

Fig 3

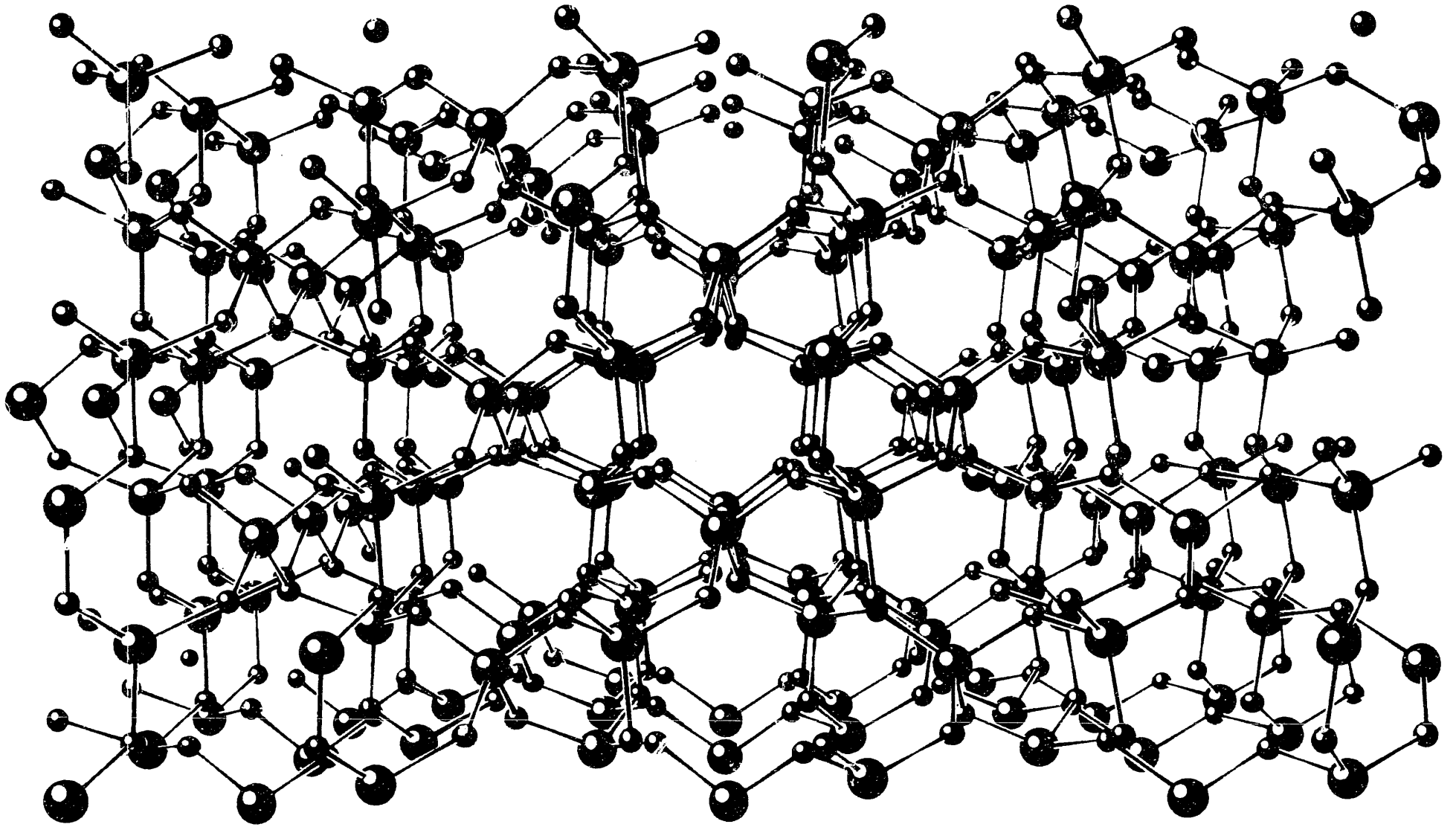

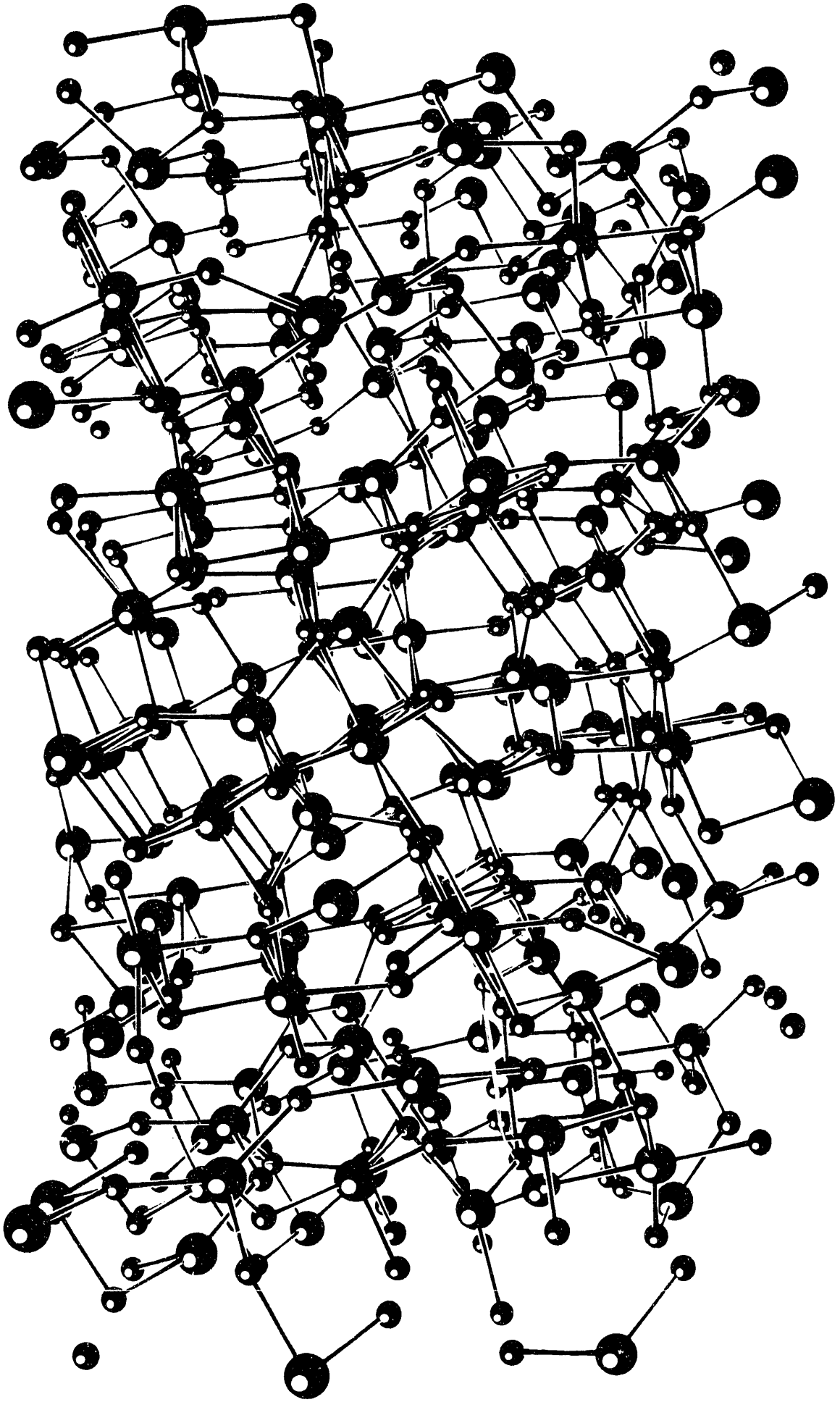

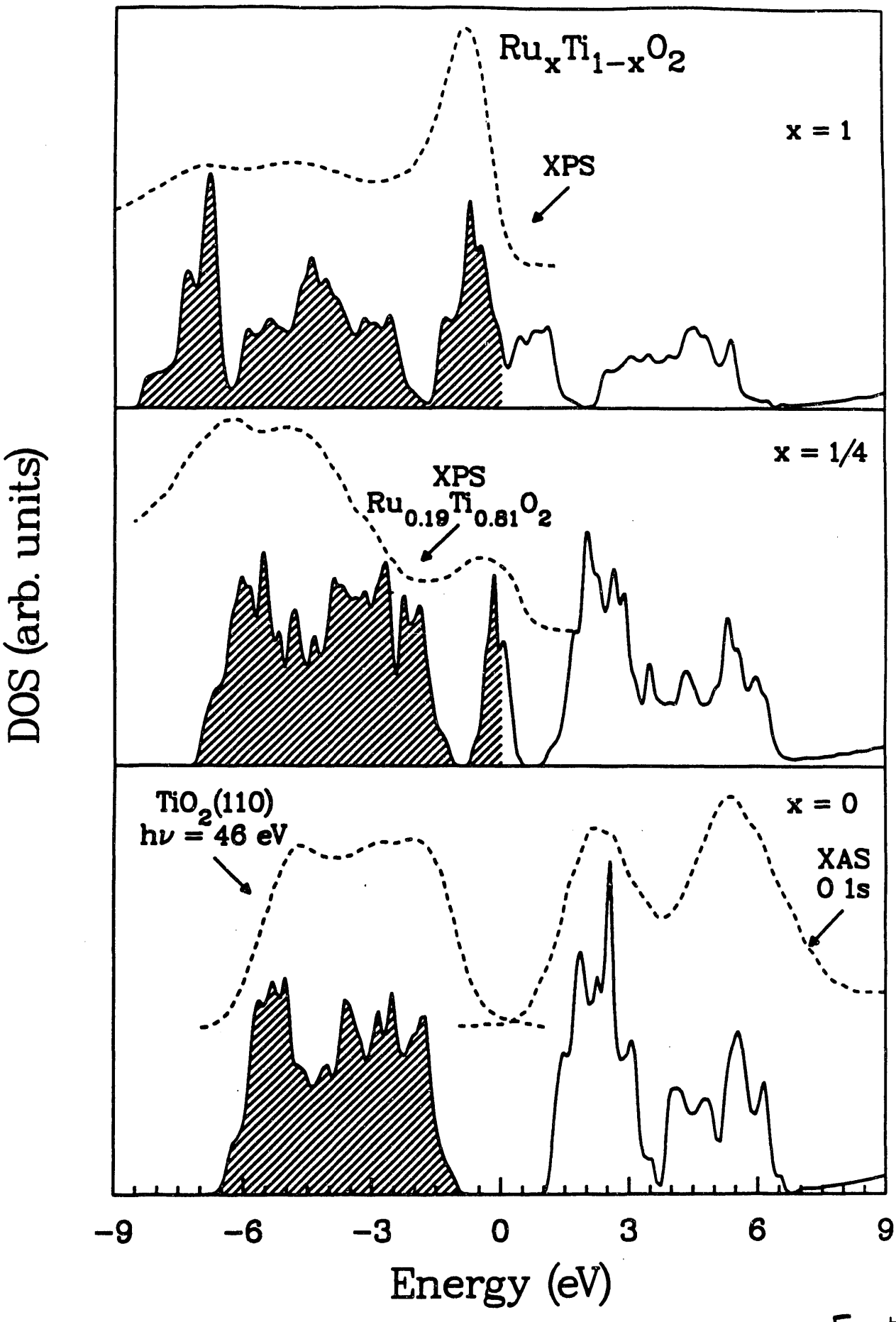
$Ru_xTi_{1-x}O_2$
x = 1
XPS
x = 1/4
XPS
$Ru_{0.19}Ti_{0.81}O_2$
TiO_2(110)
hν = 46 eV
x = 0
XAS
O 1s
DOS (arb. units)
−9
−6
−3
0
3
6
9
Energy (eV)

Fig. #6

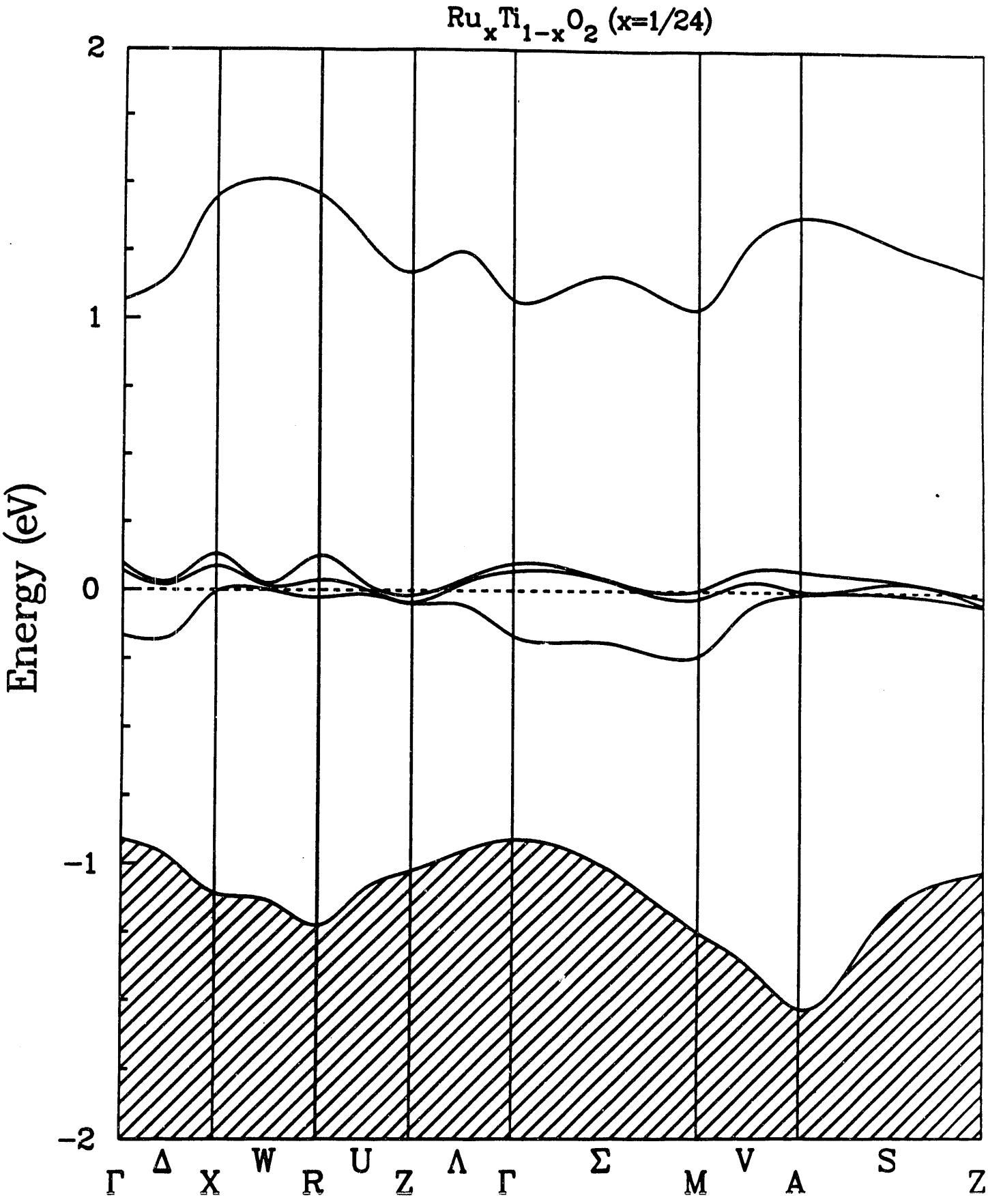

Fig. #7

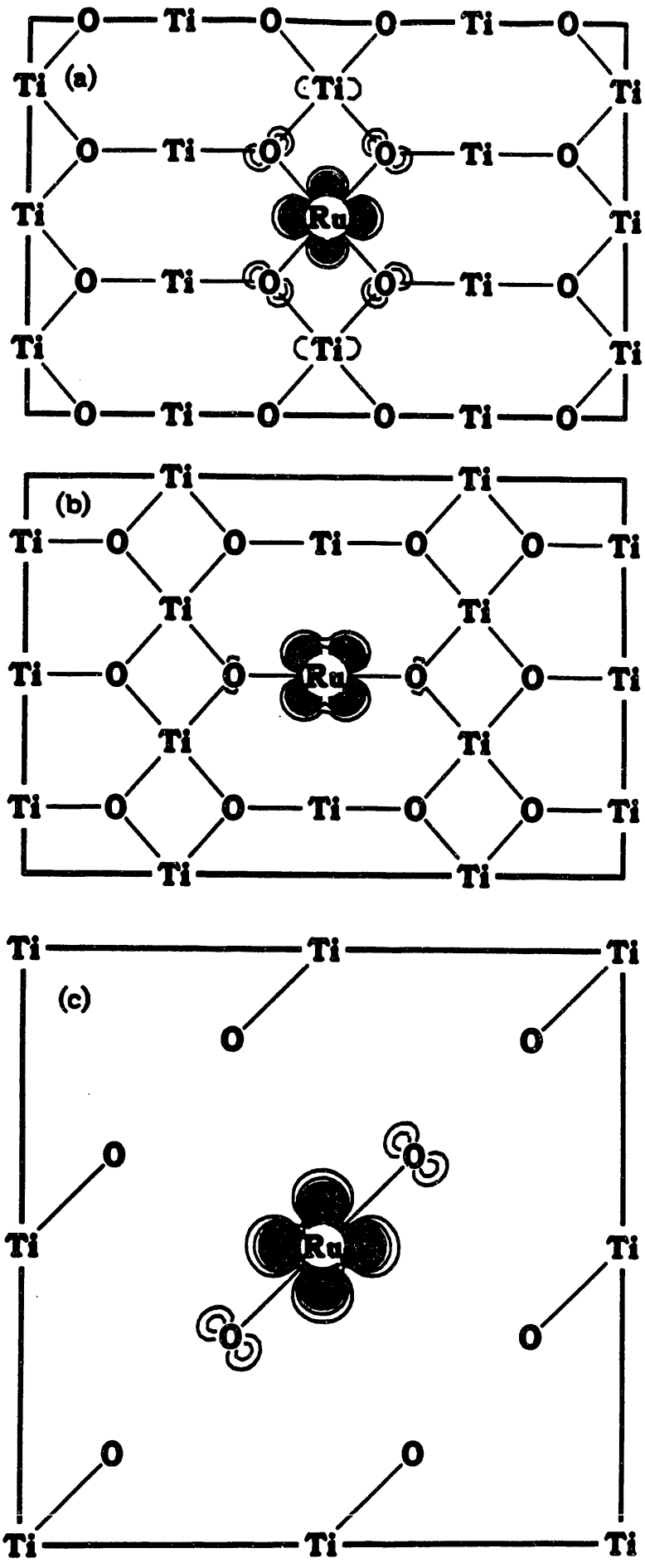

Fig. #8

3 Publications resulting from this grant

Publications in referred journals:

1. "Chemical Reactivity and Covalent/Metallic Bonding of Si_n^+ (n=11-25) Clusters," J.R. Chelikowsky and J.C. Phillips, Phys. Rev. Lett.**63**, 1653 (1989).

2. "Surface and Thermodynamic Interatomic Force Fields for Silicon Clusters and Bulk Phases," J.R. Chelikowsky, and J.C. Phillips, Phys. Rev. B **41**, 5735 (1990).

3."Interatomic Potentials and the Structural Properties of Silicon Dioxide Under Pressure,"J.R. Chelikowsky, H.E. King Jr., and J. Glinnemann, Phys. Rev. B **41**,10866 (1990).

4."The Structure of Silicon and Silicon Dioxide from Interatomic Potentials," J.R. Chelikowsky and K. Glassford, Materials Research Society Symp. Proc. **193**, 65 (1990).

5."Electronic Structure and Structural Properties of Titanium Dioxide in the Rutile Structure," K.M. Glassford, N. Troullier, J.L. Martins and J.R. Chelikowsky, Solid State Commun. **76**, 635 (1990).

6."Structural Properties of α-Quartz Near the Amorphous Transition," J.R. Chelikowsky, H.E. King, Jr., N. Troullier, J.L. Martins and J. Glinnemann, Phys. Rev. Lett. **65**, 3309 (1990).

7."Interatomic Force Fields for the Structure of Defects in Silicon, K.M. Glassford, J.R. Chelikowsky and J.C. Phillips, Phys. Rev. B **43**, 14557 (1991).

8."Interatomic Force Fields for Silicon Microclusters," J.R. Chelikowsky, K.M. Glassford and J.C. Phillips, Phys. Rev. B **44**, 1538 (1991).

9. "Pressure Dependence of the Structural Properties of α-Quartz Near the Amorphous Transition," J.R. Chelikowsky, N. Troullier, J.L. Martins, and H.E. King, Jr., Phys. Rev. B **44**, 489 (1991).

10. "Structural Properties of SiO_2 in the Stishovite Structure," N. Keskar, N. Troullier, J.L. Martins and J.R. Chelikowsky, Phys. Rev. B**44**, 4081 (1991).

11."Electronic Properties of α-Quartz Under Pressure," N. Binggeli, N. Troullier, J.L. Martins and J.R. Chelikowsky, Phys. Rev. B**44**, 4771 (1991).

12."Structural Transformations of Quartz at High Pressures," N. Binggeli and J.R. Chelikowsky, Nature**353**, 344 (1991).

13. "Optical Properties of Titanium Dioxide in the Rutile Structure," K.M. Glassford and J.R. Chelikowsky, Phys. Rev. B**45**, 3874 (1992).

14."Nucleation of C_{60} Clusters," J.R. Chelikowsky, Phys. Rev. Lett. **45**, 12062 (1992).

15. "Structural Properties of Nine Silica Polymorphs," N. Keskar and J.R. Chelikowsky, Phys. Rev. B **46**, 1 (1992).

16. "Structural and Electronic Properties of Titania" K.M. Glassford and J.R. Chelikowsky, Phys. Rev. B **46**, 1284 (1992).

17. "Simulation of Si Clusters via Langevin Molecular Dynamics with Quantum Forces," N. Binggeli, J.L. Martins and J.R. Chelikowsky, Phys. Rev. Lett. **68**, 2956 (1992).

18. "Negative Poisson Ratios in Crystalline SiO_2 from First-Principles Calculations," N. Keskar and J.R. Chelikowsky, Nature **358**, 222 (1992).

19. "Nucleation of C_{60} Clusters via Langevin Molecular Dynamics," J.R. Chelikowsky,

Phys. Rev. B **45**, 12062 (1992).

20. "Structural and Electronic Properties of RuO_2," K.M. Glassford and J.R. Chelikowsky, Phys. Rev. B (in press).

20."Elastic Instability in α-quartz Under Pressure," N. Binggeli and J.R. Chelikowsky, Phys. Rev. Lett. **69**, 2220 (1992).

21. "First Principles Methods for Structural Trends in Oxides: Applications to Crystalline Silica," J.R. Chelikowsky, N. Binggeli and N. Keskar, J. of Compounds and Alloys, (in press).

22. "Elastic Instabilities and Amorphization of Crystalline Silica Under Pressure," J.R. Chelikowsky and N. Binggeli, Mat . Res. Soc. Symp. Proc. **291**, (1993) .

23. "Electronic Structure of TiO_2:Ru," K.M. Glassford and J.R. Chelikowsky, Phys. Rev. B (in press).

24. "Doing Materials Science with a Supercomputer: On the Road to 1000 Atom Systems," J.R. Chelikowsky and N. Binggeli, Comput. Mat. Sci. (submitted).

25. "Anomalous Elastic Behavior in Crystalline Silica," N.R. Keskar and J.R. Chelikowsky, Phys. Rev. (submitted).

Book Chapters:

1. "Ab initio Pseudopotentials for Semiconductors," J.R. Chelikowsky and M.L. Cohen, *Handbook on Semiconductors*, 2nd Edition, ed. P. Landsberg, (Elsevier, 1992), Vol.1, p. 59.

END

DATE
FILMED
7/27/93